Polarization coherent anti-Stokes Raman scattering microscopy

Ji-Xin Cheng, Lewis D. Book, and X. Sunney Xie

Department of Chemistry and Chemical Biology, Harvard University, 12 Oxford Street, Cambridge, Massachusetts 02138

Received March 28, 2001

We report polarization coherent anti-Stokes Raman scattering (P-CARS) microscopy that allows vibrational imaging with high sensitivity and spectral selectivity. The nonresonant background signals from both Raman scatterers and the solvent are efficiently suppressed in P-CARS microscopy. We demonstrate P-CARS imaging of unstained cells based on the contrast of the protein amide I band. © 2001 Optical Society of America

OCIS codes: 300.6230, 110.0180, 180.6900, 190.4380.

Multiphoton microscopy based on coherent anti-Stokes Raman scattering (CARS) is becoming a powerful method for vibrational imaging. The vibrational contrast mechanism in CARS microscopy is based on the fact that the CARS signal is resonantly enhanced when the frequency difference between the pump and Stokes beams coincides with the frequency of a Raman-active vibration. After the initial work by Duncan *et al.*,[1,2] the achievement of three-dimensional CARS imaging[3] in 1999 has stimulated many developments in CARS microscopy, which include the use of near-infrared picosecond beams,[4,5] collinear epidetection geometry,[5,6] BOXCARS geometry,[7] and theoretical work on nonlinear coherent microscopy.[6,8]

CARS signals are much stronger than spontaneous Raman signals with the same average excitation power.[9] The major drawback of CARS microscopy is the existence of a nonresonant background that results from electronic contributions to $\chi^{(3)}$.[10] The nonresonant background often dominates the CARS signal,[1,2] which, until recently, limited the detection sensitivity and impeded applications of CARS microscopy. To improve the sensitivity, one needs to reduce the nonresonant background.

The signal-to-background ratio has been significantly improved by replacement of visible laser pulses[1] with near-infrared pulses[3] because the latter allow one to avoid two-photon electronic resonance.[5] Further improvement has been obtained by use of near-infrared excitation pulses with narrow spectral widths.[5] Recently, it was demonstrated that the epidetection scheme could efficiently reduce the solvent background and improve the sensitivity.[5,6]

A general way to suppress the nonresonant background is to make use of the polarization difference between the resonant and nonresonant CARS fields. Polarization coherent anti-Stokes Raman scattering spectroscopy (P-CARS) was demonstrated in the late 1970s.[11,12] In this Letter we demonstrate that polarization CARS microscopy provides high vibrational contrast by suppressing the nonresonant background from both the solvent and the Raman scatterer.

The theory of P-CARS has been described elsewhere.[12,13] Briefly, consider a pump beam at frequency ω_P and a Stokes beam at frequency ω_S propagating along the z axis. The pump beam is linearly polarized along the x axis, and the Stokes beam is linearly polarized along a direction at an angle of ϕ relative to the x axis, as shown in Fig. 1(a). Suppose that $\omega_P - \omega_S$ is resonant with a molecular vibration. In this case the interaction of the incident beams with the sample induces a third-order polarization that contains a nonresonant part, P^{NR}, and a vibrationally resonant part, P^{R}. The x and y components of P^{NR} can be written as

$$P_x^{\mathrm{NR}} = 3\chi_{1111}^{\mathrm{NR}} E_P^2 E_S^* \cos\phi\,,$$
$$P_y^{\mathrm{NR}} = 3\chi_{2112}^{\mathrm{NR}} E_P^2 E_S^* \sin\phi\,. \quad (1)$$

Similarly, the x and y components of the resonant part can be written as

$$P_x^{\mathrm{R}} = 3\chi_{1111}^{\mathrm{R}} E_P^2 E_S^* \cos\phi\,,$$
$$P_y^{\mathrm{R}} = 3\chi_{2112}^{\mathrm{R}} E_P^2 E_S^* \sin\phi\,. \quad (2)$$

In the absence of any electronic resonance in the system, χ^{NR} is a real quantity that is independent of frequency. In this case the depolarization ratio of the nonresonant CARS field, $\rho_{\mathrm{NR}} = \chi_{2112}^{\mathrm{NR}}/\chi_{1111}^{\mathrm{NR}}$, assumes a value of 1/3.[13] P^{NR} is therefore linearly polarized with an angle of α relative to the x axis,

$$P^{\mathrm{NR}} = 3\chi_{1111}^{\mathrm{NR}} E_P^2 E_S^* \cos\phi/\cos\alpha\,, \quad (3)$$

where the angle α is related to ϕ by $\tan\alpha = \rho_{\mathrm{NR}} \tan\phi$.

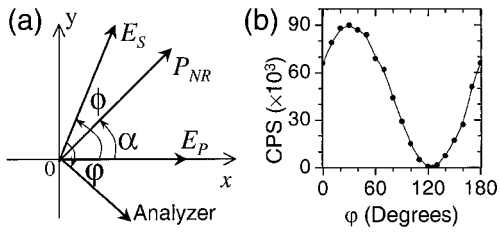

Fig. 1. (a) Polarization vectors of the pump and the Stokes fields, the nonresonant CARS signal, and the analyzer polarizer. (b) Nonresonant CARS signal [counts/s (CPS)] from a water–glass interface as a function of angle φ. The ratio of the maximum counts at $\varphi \sim 30°$ to the minimum counts at $\varphi \sim 120°$ is 600:1.

0146-9592/01/171341-03$15.00/0

The nonresonant background can be removed by placement of an analyzer before the detector, with polarization perpendicular to P^{NR}. The total projection of the two components of P^{R} [Eq. (2)] along the direction perpendicular to P^{NR} can be written as

$$P_{\perp} = 3E_P^2 E_S^* \chi_{1111}^{\mathrm{R}} (\cos\phi \sin\alpha - \rho_{\mathrm{R}} \sin\phi \cos\alpha) . \tag{4}$$

Here, $\rho_R = \chi_{2112}^{\mathrm{R}}/\chi_{1111}^{\mathrm{R}}$ is the depolarization ratio of the resonant CARS field. ρ_{R} is equal to the spontaneous Raman depolarization ratio in the absence of electronic resonance.[13]

Theoretically, the signal from $P_{\perp}$ is background free. In practice, there exists a residual background because of the birefringence of the optics in the beam path and the scrambling of polarization at the tight focus. The extinction ratio is defined as the ratio of the maximum to minimum signals obtained by rotation of the analyzer. Assuming that the extinction ratio is r for the nonresonant background, the vibrational contrast is given by

$$rP_{\perp}^2/(P^{\mathrm{NR}})^2 = r(\chi_{1111}^{\mathrm{R}}/2\chi_{1111}^{\mathrm{NR}})^2(1 - \rho_{\mathrm{R}}/\rho_{\mathrm{NR}})^2 \sin^2 2\alpha . \tag{5}$$

It is clear that the vibrational contrast is maximized when α equals 45°. The optimal value for the angle ϕ is then 71.6°, according to the relation $\phi = \tan^{-1}(3 \tan\alpha)$. P-CARS microscopy can be applied to vibrational imaging by use of Raman bands with $\rho_{\mathrm{R}} \neq \rho_{\mathrm{NR}}$. For example, if $\rho_{\mathrm{R}} = 0$ the contrast can be improved by $r/4$ times compared with the case with parallel-polarized excitation beams.

The schematic of our P-CARS microscope is shown in Fig. 2. The pump and the Stokes beams are two synchronized 5-ps near-infrared pulse trains. Details of the laser system can be found elsewhere.[5] Both the pump and the Stokes beams are linearly polarized. The polarization direction of the pump beam is adjustable with a half-wave plate. The angle ϕ is set at 71.6° in our experiment. A quarter-wave plate is used to compensate for the birefringence in the pump field that is induced by the dichroic mirror. The analyzer is installed on a rotation mount.

The extinction ratios of both the pump and the Stokes beams measured at the detector are ~120:1. However, a higher extinction ratio (600:1) of the nonresonant CARS signal from the water–glass interface is experimentally seen in evaluation of the polarization of the signal, as shown in Fig. 1(b). This is because CARS is a third-order nonlinear process, and thus the depolarized components of the incident fields contribute little to the CARS signal.

Figure 3(a) shows the P-CARS spectrum for a 1-μm polystyrene bead at the water–glass interface. The two P-CARS bands at 1600 and 1582 cm^{-1} are coincident with the Raman bands. A high signal-to-background ratio (10:1) is obtained, indicating that the nonresonant signals from the bead and its surrounding medium are effectively suppressed. The P-CARS signal from the weak Raman band of water near 1620 cm^{-1} is not detectable in our experiment. The CARS spectrum of polystyrene taken with parallelly polarized pump and Stokes beams is also shown for comparison. A large nonresonant background is present, with a dip at 1608 cm^{-1} that arises from the

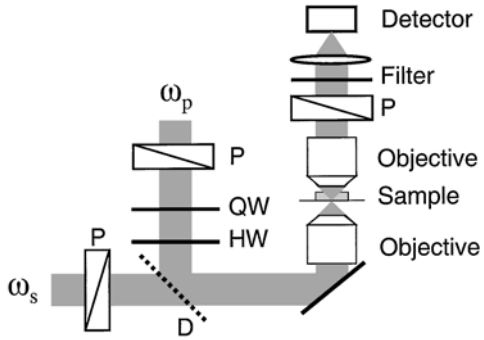

Fig. 2. Schematic of the P-CARS microscope: P, polarizer; HW, half-wave plate; QW, quarter-wave plate; D, dichroic mirror. The lower objective is a water objective (N.A., 1.2; Olympus). The upper objective is an oil objective (N.A., 1.4; Nikon). The detector is an avalanche photodiode connected to a digital counter (SRS, SR620) and a homemade data-acquisition system.

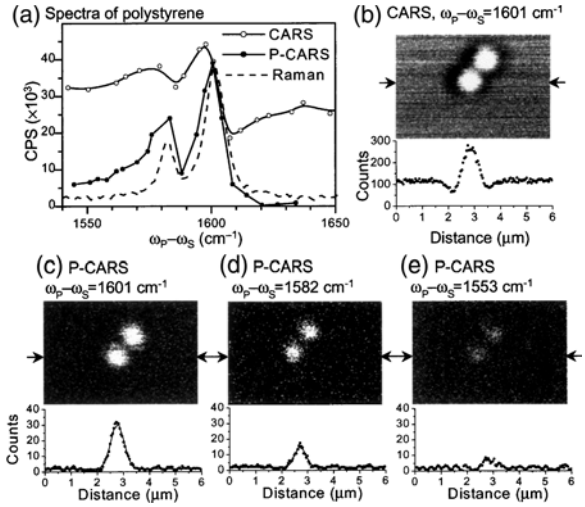

Fig. 3. (a) P-CARS spectrum of a 1-μm polystyrene bead spin coated on a coverslip and covered with water, taken with a pump power of 350 μW and a Stokes power of 250 μW at a repetition rate of 50 kHz. The CARS spectrum of a polystyrene film was taken with a pump power of 780 μW and a Stokes power of 390 μW at a repetition rate of 100 kHz. The pump frequency was fixed at 13 325 cm^{-1}. The Stokes frequency was tuned from 11 691 to 11 780 cm^{-1}. The P-CARS signals are multiplied by a factor of 30. The spontaneous Raman spectrum of polystyrene was recorded on a Raman spectrometer (Jobin Yvon-Spex, LabRam). (b) CARS image of 1-μm polystyrene beads spin coated on a coverslip and covered with water. The pump and Stokes powers were 0.6 and 0.3 mW, respectively, at a repetition rate of 400 kHz. (c)–(e) P-CARS images of the same polystyrene beads with $\omega_P - \omega_S$ tuned to 1601, 1582, and 1553 cm^{-1}. The pump and Stokes powers were 1.4 and 0.7 mW, respectively, at a repetition rate of 400 kHz. The acquisition time was 1.0 min for each image in (b)–(e). Shown below the images are the intensity profiles across the lines indicated by the arrows.

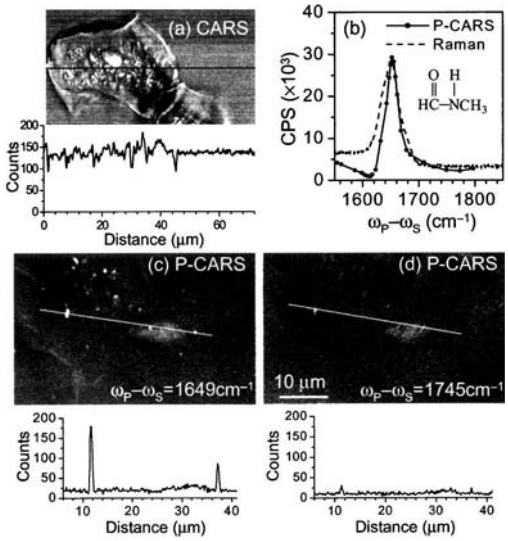

Fig. 4. (a) CARS image of an epithelial cell without polarization-sensitive detection, $\omega_P-\omega_S$ was tuned to the protein amide band. The pump and Stokes powers were 0.4 and 0.2 mW at a 400-kHz repetition rate. The acquisition time was 4 min. (b) P-CARS and Raman spectra of pure *N*-methylacetamide liquid. The P-CARS spectrum was recorded with average pump and Stokes powers of 1.6 and 0.8 mW at a pulse repetition rate of 400 kHz. (c) P-CARS image of an unstained epithelial cell with $\omega_P-\omega_S$ tuned to 1650 cm^{-1}. (d) Same as (c) but with $\omega_P-\omega_S$ tuned to 1745 cm^{-1}. The pump and Stokes powers were 1.8 and 1.0 mW, respectively, at a repetition rate of 400 kHz. The acquisition time was 8 min. Shown below the images are the intensity profiles across the lines indicated in the images.

interference between the resonant and nonresonant signals.[9]

Figure 3(b) shows a CARS image of 1-μm polystyrene beads in water, taken without polarization-sensitive detection. A large background signal from the water can be seen from the intensity profile shown below the image. Figures 3(c)–3(e) show P-CARS images of the same beads in water with $\omega_P-\omega_S$ tuned to 1601, 1582, and 1553 cm^{-1}, respectively. When $\omega_P-\omega_S$ is tuned to the 1601-cm^{-1} band, a high signal-to-background ratio can be seen from the intensity profile across the bead. Tuning $\omega_P-\omega_S$ to 1582 cm^{-1} results in a peak intensity that is half of that in Fig. 3(c), which is consistent with the P-CARS spectrum [Fig. 3(a)] of polystyrene. The signal almost disappears when $\omega_P-\omega_S$ is tuned away from any vibrational resonance. The results presented above demonstrate that P-CARS microscopy allows vibrational imaging with high contrast.

Figure 4(a) shows a typical CARS image of an epithelial cell recorded without polarization-sensitive detection. $\omega_P-\omega_S$ is tuned to a region in which the protein amide band resides. A large background signal from water can be seen. Moreover, there is little change of contrast when $\omega_P-\omega_S$ is tuned, indicating the nonresonant signal from the cellular components overwhelms the resonant CARS signal. In contrast, P-CARS microscopy is capable of vibrational imaging of proteins with a high contrast. Figure 4(b) shows the P-CARS spectrum of the amide I band of *N*-methylacetamide. *N*-methylacetamide is a model compound containing the characteristic amide vibration of peptides and proteins. The amide I band at 1652 cm^{-1} shows a high signal-to-background ratio. P-CARS imaging of unstained epithelial cells based on the amide I band is demonstrated in Figs. 4(c) and 4(d). When $\omega_P-\omega_S$ is tuned to the protein amide I band at 1650 cm^{-1}, strong signals from small features in the cytoplasm are observed [Fig. 4(c)]. These bright features might be mitochondria that are rich in proteins and will be the subject of future studies. The nucleus shows a weaker signal. The vibrational contrast was largely diminished when $\omega_P-\omega_S$ was tuned away from the amide I band to 1745 cm^{-1} [Fig. 4(d)]. This result indicates that the main contribution to the contrast is the resonant CARS signal of the amide I band.

In conclusion, polarization CARS microscopy provides high vibrational contrast by suppressing the nonresonant background from the Raman scatterer and its surrounding medium. The present work demonstrated high-sensitivity vibrational imaging of live cells based on the amide band of proteins. The average excitation power (~2 mW) employed is tolerable by live cells. This methods can also be used for imaging of various chemical species in heterogeneous materials.

This research was supported by a start-up fund at Harvard University. The authors thank Andreas Volkmer and Erik Sánchez for technical help. Sunney Xie's e-mail address is xie@chemistry.harvard.edu.

References

1. M. D. Duncan, J. Reintjes, and T. J. Manuccia, Opt. Lett. **7,** 350 (1982).
2. M. D. Duncan, J. Reintjes, and T. J. Manuccia, Opt. Eng. **24,** 352 (1985).
3. A. Zumbusch, G. R. Holtom, and X. S. Xie, Phys. Rev. Lett. **82,** 4142 (1999).
4. M. Hashimoto, T. Araki, and S. Kawata, Opt. Lett. **25,** 1768 (2000).
5. J. X. Cheng, A. Volkmer, L. D. Book, and X. S. Xie, J. Phys. Chem. B **105,** 1277 (2001).
6. A. Volkmer, J.-X. Cheng, and X. S. Xie, Phys. Rev. Lett. **87,** 023901 (2001).
7. M. Müller, J. Squier, C. A. de Lange, and G. J. Brakenhoff, J. Microsc. (Oxford) **197,** 150 (2000).
8. E. O. Potma, W. P. D. Boeij, and D. A. Wiersma, J. Opt. Soc. Am. B **17,** 1678 (2000).
9. M. D. Levenson and S. S. Kano, *Introduction to Nonlinear Laser Spectroscopy* (Academic, San Diego, Calif., 1988), p. 148.
10. S. Maeda, T. Kamisuki, and Y. Adachi, in *Advances in Non-linear Spectroscopy*, R. J. H. Clark and R. E. Hester, eds. (Wiley, New York, 1988), pp. 253–297.
11. S. A. Akhmanov, A. F. Bunkin, S. G. Ivanov, and N. I. Koroteev, JETP Lett. **25,** 416 (1977).
12. J.-L. Oudar, R. W. Smith, and Y. R. Shen, Appl. Phys. Lett. **34,** 758 (1979).
13. R. Brakel and F. W. Schneider, in *Advances in Nonlinear Spectroscopy*, R. J. H. Clark and R. E. Hester, eds. (Wiley, New York, 1988), pp. 149–192.